IJL, Issue 1, Vol. 24, 2025
https://doi.org/10.31900/ijl.v24i1.489

Research Article

Highly Sensitive Refractive Index Sensor Based on Dual Peak Plasmonic Tapered D-shaped PM-PCF Coated with Gold Nano-Structures

Suaad Sahib Hindal[1,2,*], Zainb F. Al-Bawai[1] , Aseel I. Mahmood[2]

[1] *Institute of Laser for Postgraduate Studies, University of Baghdad*
[2] *Scientific Research Commission, Ministry of Higher Education& Scientific Research, Baghdad, Iraq*
* *Email address of the Corresponding Author: suad.saheb2101p@ilps.uobaghdad.edu.iq*

Article history: Received: 20 Jul. 2024; Revised: 3 Sept. 2024; Accepted: 17 Sept. 2024; Published online 15 Jun. 2025

Abstract

This paper uses the finite element method (FEM) to study a Surface Plasmon Resonance (SPR) refractive index sensor based on D-shaped Polarization Maintain Photonic Crystal Fiber (PM-PCF). A chemically stable plasmonic material, gold (Au), with hemispherical structures having a radius of 50 nm, is applied to the surface of a D-shaped sensor to create the surface plasmon resonance (SPR) effect, enabling this SPR sensor to detect variation in the surrounding analyte refractive index (RI). The resonance condition will change when the refractive index of the targeted analyte changes, leading to a certain shift in the loss peak. Two resonant peaks are observed, one located in the visible part of the spectrum, and the second in the near-infrared region. Our suggested design offers a high wavelength sensitivity (WS) of 5176 nm/RIU and the spectral resolution for this sensor is 1.93 x 10^{-5} RIU, for y-polarization. For x-polarization, the wavelength sensitivity of the 1st and 2nd peaks are 1058 nm/RIU and 3764 nm/RIU, respectively. The spectral resolution for the 1st and 2nd peaks is 9.45x 10^{-5} RIU and 2.65x 10^{-5} RIU, respectively in the high sensing range of 1.34 to 1.41 RIU. The results show that this improves the sensor's ability to detect the refractive index. The proposed SPR sensor design has high sensitivity, high resolution, and high linearity, a promising result that could be used in environmental monitoring, biological detection, physical sensors, and chemical analysis.

Keywords: D-shape PM-PCF; Finite Element Method (FEM); Polarization Maintaining Photonic Crystal Fiber (PCF); Refractive Index Sensor; Surface Plasmon Resonance (SPR)..

1. Introduction

Optical fibers have become an ideal option for sensing applications due to their precision, compact size, high sensitivity, and remote sensing [1]. There exist many types of optical fibers like single-mode fibers [2], multimode fibers [3], No-Core Fibers [4], photonic crystal fibers (PCFs) [5], and nanostructured fibers

[6]. Various sensing approaches are employed in optical fibers such as surface plasmon resonance (SPR), Bragg gratings, interferometers, long-period gratings, and fluorescence [7].

The Fabry-Perot (FP) interferometer usually comprises two mirrors with high reflectivity. The incident light beam reflects multiple times between these mirrors, leading to multiple-beam interference [8]. Fabry-Perot (FP) interferometric sensors stand out among the many optical fibers proposed because they are simple, accurate, adaptable, responsive, and resistant to environmental noise [9].

The working principles of optical fiber FP interferometer sensors are primarily explained by the propagation phase shift equation φ in the interferometer, where $\varphi = \frac{2\pi}{\lambda} \Delta$ (with Δ representing the optical path difference (OPD) and λ denoting the free-space optical wavelength). When a disturbance is introduced to the sensor, the phase difference is affected due to the variation in the OPD of the interferometer. By observing the shift in the phase or wavelength spectrum, the sensing parameter applied to the optical fiber FP interferometer sensor can be accurately determined [10].

Thin film technology is essential in fiber optic sensors by coating reflective surfaces inside the FP cavity or on the fiber surface, which allows for the measurement of specific physical parameters [8].

SPR sensors based on optical fiber garner significant research attention in environmental monitoring, biomedical, food detection, etc., due to features like real-time monitoring, high sensitivity, wide operated wavelength range, and label-free detection [11]. The D- shape plasmonic refractive index (RI) sensors are a typical part of these sensors, which have been functionalized for responding indirectly to diverse factors such as liquid/gas concentration, temperature, and various biological and physicochemical parameters [11, 12]. The performance of these sensors based on an optical fiber is generally evaluated in terms of the following key parameters: sensitivity, resolution and FOM.

The physical-optical phenomenon including excitation of oscillations in electron density at metal-dielectric interfaces when exposed to p-polarized light waves is called Surface Plasmon Resonance (SPR) [12, 13]. This excitation leads to a sharp loss in the propagation spectrum. The peak of the loss is called the resonance frequency or resonance wavelength, which is highly sensitive to the surrounding RI changes [14]. This characteristic makes it widely utilized in biomedical, biological, and chemical monitoring applications [12, 15].

The sensor's performance depends mainly on the plasmonic materials [16]. and Silver (Ag) [17], Gold (Au) [18], Aluminum (Al) [19], and Copper (Cu) [17], etc., are popular plasmonic materials [20]. Silver presents a high resonance peak [21], but at the same time, it experiences oxidation problems when exposed to water. Gold is primarily preferred as a plasmonic material [16, 22]; because of its biocompatibility, chemical stability, and gold exhibits strong surface plasmon resonance in the visible and near-infrared (NIR) spectrum. This makes it highly effective for SPR applications that operate in these wavelength ranges, which are commonly used in optical sensing. Therefore, gold is chosen as the plasmonic material in this work.

The sensitivity of optical fiber sensors is crucial for improving their capability to detect small variations in the surrounding refractive index.In other words, it allows for detecting low analyte concentration and thus enhances the SPR sensor performance [23]. There are many strategies to reach this goal like choosing the type of plasmonic material to get strong SPR resonance. Metal thickness is also a crucial factor. In addition, the shape of nanoparticle material which is used as a plasmonic layer [24]. Different structures of SPR sensors using photonic crystal fibers (PCFs) have been suggested to address the limitations found in multiple optical fiber SPR sensors [25] and fiber gratings [26] which displays poor sensitivity. In this case, the surface plasmons (SPs) are activated by the evanescent wave that passes through the metal film. Photonic crystal fiber provides significant flexibility by modifying the arrangement of air holes in the core and cladding regions. Moreover, PCFs are small, and compact, making them precise for creating miniaturized devices for remote sensing applications. Various structures of PCF have been suggested for the sensors based on SPR, each offering different sensing capabilities and detection ranges [27].

Plasmonic sensors based on PCFs have many applications in measurements and detection. For example but not limited to Refractive Index Sensor (RI)[28], Biomedical applications [29], magnetic field [30], Temperature[31] and many others.

Fiber optic geometry is also a very important factor in enhancing the SPR sensor sensitivity, geometries were introduced like U-shape [32], double side polished U- shape [33], flat tip [34], and D-shape [35].

This type of photonic device has received significant interest from the scientific community. Below, we will mention some of the most recently published work.

In 2020, Meng et al. [36] proposed a D-shaped SPR sensor with dual loss peaks, reaching a maximum sensitivity of 18,900 nm/RIU and 17,500 nm/RIU, respectively of the primary and secondary peaks, within the RI range of (1.35-1.38). The spectral resolutions are 5.291×10^{-6} and 5.714×10^{-6} RIU, respectively. Alok K. Paul et al [27] designed and evaluated of an SPR sensor in a photonic crystal fiber (PCF) platform, where graphene is applied externally to enhanced sensing performance for an aqueous solution. The proposed sensor performance was evaluated using the finite element method-based simulation tool COMSOL Multiphysics. The simulation results indicate that the proposed sensor exhibits identical linear characteristics and achieves a very high figure of merit (FOM) of 2310.11 RIU^{-1} in the very low detection limit of 10^{-3}. The average wavelength sensitivity is 2000 nm/RIU for the analyte RI ranging from 1.331 to 1.339. Mumtaz et al. in 2022 [37], presented an SPR sensor based on optical fiber with extremely high sensitivity for simultaneous dual-parameter measurement. The SPR sensor utilizes a D-shaped fiber coated with a nanolayer of Silver (Ag) and Hematite (α-Fe2O3). This sensor demonstrates an exceptionally high refractive index sensitivity of 8,518 nm/RIU within the RI range of 1.33 to 1.40. The SPR performance indicates its potential for various dual-parameter sensing applications. Ruan et al [38] designed an arc-shaped PCF with high refractive index sensitivity. They use the finite element method (FEM) to create the analyte channel of an open arc-shaped at the top of the fiber, facilitating the detection of the analyte's RI. To stimulate mode coupling, a gold layer is applied inside the arc-shaped structure. The influence of changing the diameters of the air hole rings and thickness of the metallic layer on sensor performance is done. The sensor's maximum sensitivity is 24900 nm/RIU; the spectral resolution is 4.01×10^{-6} RIU; and the figure of merit (FOM) is 661.71 RIU^{-1}. Yu Ying et al [39]designed and evaluated a dual−core D-shaped PCF surface plasmon resonance sensor, which was coated with gold grating using the FEM method. They examined how various PCF structural parameters such as small and large air holes and polishing depths along with grating parameters like grating duty, heights, and periods, influence the sensor's performance. The findings indicate that both the grating and dual-core design are crucial in enhancing the sensor's capabilities. The proposed sensor achieves an average wavelength sensitivity of 994.5 nm/RIU as the analyte's refractive index increases from 1.33 to 1.37. Furthermore, a maximum amplitude sensitivity of 181.049 RIU^{-1} is reported. The resolution of the dual-feature interrogation is determined to be 2.03×10^{-6} RIU, which is better than the wavelength and amplitude interrogations. In 2024, Chen et al. proposed a novel, dual-functional, ultra-sensitive sensor using a D-shaped microchannel PCF for temperature and refractive index (RI) sensing. Its high sensitivity is achieved by incorporating magnesium fluoride (MgF2) and gold (Au) as plasmonic materials within the channel of a micro-rectangular shape. These simulations reveal a wide detection range, spanning refractive index values from 1.27 to 1.43. The sensor achieves peak sensitivities of 31,800 nm/RIU, a maximum resolution of 3.14×10^{-6} RIU, and a FOM of 211.07 RIU^{-1} in the analyte RI range of 1.27-1.43 [40].

This research paper presents a refractive index (RI) sensor based on a D-shape PM_PCF plasmonic configuration. Gold hemisphere structure is used as plasmonic material. The confinement loss spectrum characteristics of the proposed configuration are analyzed utilizing the finite element method (FEM) accompanied by perfectly matched layers absorbing boundary conditions. Sensitivity, spectral resolution, and figure of merit (FOM) are calculated to assess its sensing capability. This design introduces several enhancements: Sensitivity, Spectral Resolution and FOM, and broader applicability unlike some studies with narrow RI ranges, our design aims for a broad detection range, making it more versatile for various applications.

2. Design Considerations of the Sensor

The suggested design is studied and assessed using the Finite Element Method (FEM) within COMSOL Multiphysics (version 6.1). A two-dimensional D-shape PM-PCF is built, and the radio frequency, electromagnetic waves, and frequency domain (emw) model is selected to calculate the effective RI of core mode and SPR mode. The perfectly matched layer (PML) boundary condition is utilized in this model to enhance the absorption of the reflected light [41], the thickness of the PML layer is (T_{pml}= 2µm).
The designed model is a D-shape PM-PCF, and the dimensions and the hole structure of the PM-PCF are the same as the commercial PM-1550-01 from Thorlabs Inc. The Polarization Mode Dispersion (PMD) for this PCF fiber is typically around 0.1 ps/√km. Figure (1) shows a Scanning Electron Microscope (SEM) image of this fiber.

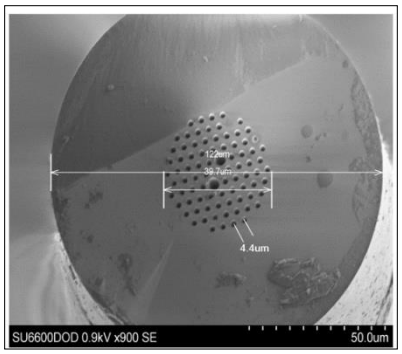

Fig. 1: SEM image of PM-1550-01-PCF

The orientation of light waves in some applications like interferometric sensors needs to be preserved. Thus, the PM-PCF which maintains the polarization state of light propagating through optical fibers, will be an excellent choice to enhance the interaction between the guided modes and the plasmonic surface. This results in higher sensitivity to changes in the refractive index of the surrounding medium. The air holes are arranged in hexagonal shape according to the SEM image, the solid core is encircled by five rows of circular holes. The bare fiber's diameter is (122) µm, while the coating's diameter is 230 µm. The diameter of the holey area which has a hexagonal symmetry is (d_H=39.7) µm, the two holes adjacent to the core have a larger diameter of (d_L=4.4) µm, and the diameter of the other holes is (d_S=2.2) µm. The pitch which is the inter-hole spacing equal to (P=4.4) µm. The same structure and dimensions of air holes are used to build the sensor in this work. The designed optical fiber is tapered to (d_T=53.64) µm diameter and polished to form the D-shape structure as shown in Figure 2. This thickness was chosen because it is the closest distance to the holes, which are filled with the analyte under study. Consequently, it achieves a strong interaction and, thus, high sensor performance. The vertical distance between the polished side of the structure to the end of the air hole rings is (V_d=26.82) µm.

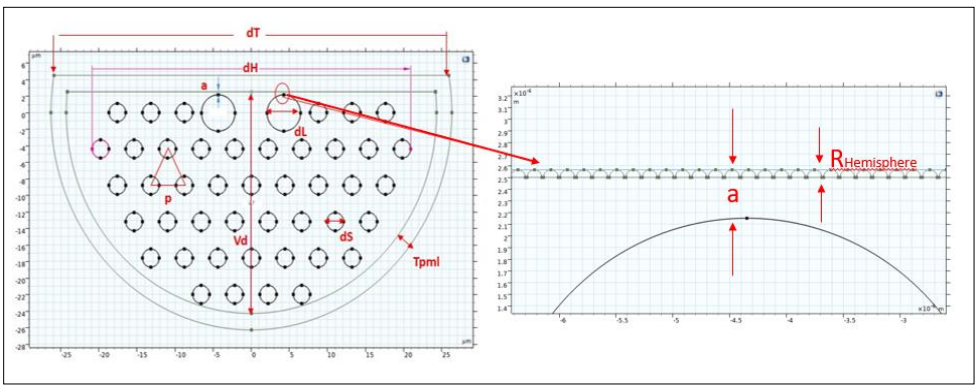

Fig. 2: The dimensions of the D-shape-PM-PCF-SPR Structure

the gold hemisphere structure of a radius (R_h=50) nm is applied above the polished designed fiber to form the plasmonic metal layer. The distance between the big hole outer diameter and the edge of the plasmonic layer is (a=0.35) µm, the distance equal to (0.4) µm it's measured with the plasmonic structure. The dimensions of the designed structure are shown in table (1).

Table 1 The designed parameter of the proposed structure

Parameter	Description	Value
dT	Tapered diameter	53.64 µm
dH	Hole's region diameter	39.7 µm
dL	The diameter of the big hole	4.4 µm
dS	The small hole diameter	2.2 µm
P	Pitch	4.4 µm
Vd	Vertical Polished distance	26.82 µm
N	No. of air hole rings	5 rings
T_{pml}	PML thickness	2 µm
$R_{Hemisphere}$	Plasmonic Hemisphere structure radius	50 nm
A	Distance from air hole and polished fiber	0.35 µm

The proposed optical fiber is made of silica (Si). The design aims to detect variations in the analyte's RI (n_a), specifically at values of (1.34, 1.35,1.36, 1.37, 1.39, 1.41) RIU. The air holes are filled with analytes RI. Figure (3) illustrates the material layout of the designed D-shape PM-PCF-SPR sensor.

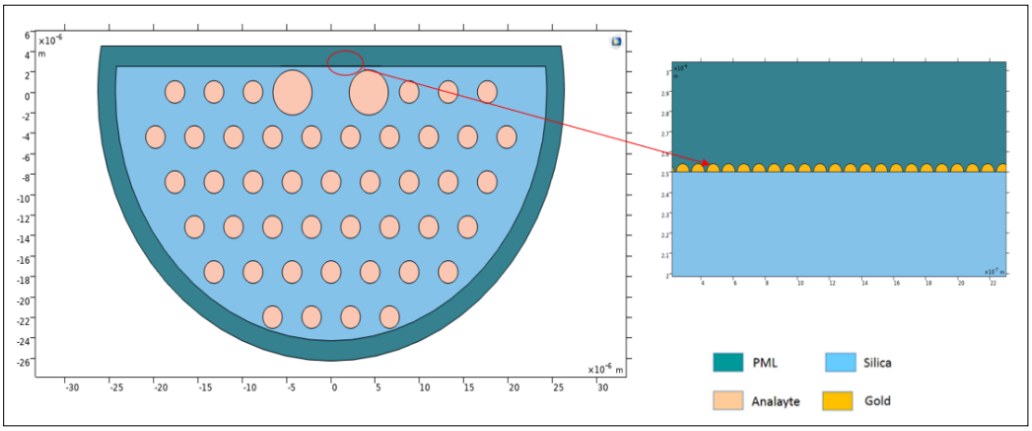

Fig. 3: Schematic illustration of the designed sensor with hemisphere plasmonic structure.

3. Numerical Method

As mentioned before, silica (SiO_2) is the background material for the sensor, and its dispersion can be expressed by the Sellmeier dispersion relation [42]:

$$n_s^2(\lambda) = 1 + \frac{B_1\lambda^2}{\lambda^2 - C_1} + \frac{B_2\lambda^2}{\lambda^2 - C_2} + \frac{B_3\lambda^2}{\lambda^2 - C_3} \qquad (1)$$

where n_s is the RI of the proposed sensor's cladding, λ is the wavelength of the incident light in µm, and the values of B_1, B_2, B_3, C_1, C_2 and C_3 coefficients in the Sellmeier equation [42] are shown in Table 2.

Table 2 Coefficients of the Sellmeier equation for silicon dioxide

B_1	B_2	B_3	C_1 (μm^2)	C_2 (μm^2)	C_3 (μm^2)
0.69616630	0.40794260	0.89747940	0.004679148260	0.01351206310	97.93400250

The plasmonic material selected for SPR excitation in this model is gold, and its permittivity (ε_{Au}) for a given wavelength is characterized by the Drude–Lorentz (DL) model [43]:

$$\varepsilon_{Au} = \varepsilon_{\infty} - \frac{\omega_D^2}{\omega(\omega + j\gamma_D)} - \frac{\Delta\varepsilon.\Omega_L^2}{(\omega^2 - \Omega_L^2) + j\Gamma_L\omega} \qquad (2)$$

Where, ω is the angular frequency, γ_D is the damping frequency, ω_D is the plasmon frequency, ε_{∞} is permittivity at high frequencies which is equal to 5.9673, and $\Delta\varepsilon = 1.09$ is the weighting factor. Oscillator strength is $\Omega_L/2\pi = 650.07\ THz$, and Lorentz's spectral width is [44]:
$\Gamma_L/2\pi = 104.86\ THz$.
The SPR sensor-based PCFs operate due to the mechanism of interactions between surface electrons of the plasmonic material and the evanescent field [45]. When light propagates with a critical angle through the sensor's surface, some leaky modes escape from the air holes array and reach the metal layer covering the sensor's polished surface. This interaction causes a generation of free electrons excited from the sensor surface, due to this interaction, the SPR effect will produce different modes of core and SPP. The resonance will be generated when the frequency of the evanescent field matches the frequency of the free electrons generated from the plasmonic layer material. This phenomenon is characterized by the confinement loss (C_L) which explains the loss in propagation, calculated using Equation (2). The C_L in dB/m given by [42]:

$$C_L = \frac{40\pi}{\ln(10)\lambda} \times Im(n_{eff}) \times 10^4 \qquad (3)$$

Where $Im(n_{eff})$ the effective RI imaginary part, and λ is the operating wavelength.

The following parameter wavelength sensitivity examines the submitted sensor performance [11], refractive index resolution [46], linearity [47], the figure of merit [16], and Birefringence [16]. The wavelength sensitivity ($S(\lambda)$) in (nm/RIU) is a method to evaluate the sensing performance of the designed sensor, and it is described by [11]:

$$S(\lambda) = \frac{\Delta\lambda_{peak}}{\Delta n_a} \qquad (4)$$

Where $\Delta\lambda_{peak}$ indicates the difference in resonance wavelength, and Δn_a represents the variation in the analyte RI.
To evaluate the sensor's detection capability, a resolution (R) parameter is introduced. This parameter is calculated in RIU as follows [46]:

$$R = \Delta n_a \frac{\Delta\lambda_{min}}{\Delta\lambda_{peak}} \qquad (5)$$

$\Delta\lambda_{min}$ represents the minimum spectral resolution (equal to 0.1 nm) for calculation [48].
Another metric for evaluating sensor performance is the figure of merit (FOM), the factor that combines sensor sensitivity ($S(\lambda)$) and full width at half maximum (FWHM), which defined as [16] :

$$FOM = \frac{m}{FWHM} \qquad (6)$$

Where m represents the slope of two adjacent resonance points, while FWHM represents the full width at half the maximum peak for each detected signal peak.
Finally, maintaining the polarization state is important in sensing. The ease of birefringence is because of the adaptable structural design and optical properties of photonic crystal fiber (PCF). The difference in the refractive index (RI) real parts of the x- and y- y-polarized core modes is defined as Birefringence (B) [16]:

$$B = \left|Re\left(n_{eff}^{x}\right) - Re\left(n_{eff}^{y}\right)\right| \qquad (7)$$

4. Simulation Results and Discussion

In this study, PM-PCF is utilized. This approach preserves the light polarization state within the optical fiber, enhancing the sensor's sensitivity to minimal variation in the surrounding refractive index (RI). Additionally, it reduces birefringence which causes undesired polarization states-related effects, thereby improving the sensor's responsiveness.
Generally, the SPR sensor functions owing to the interaction between the evanescent wave and the electrons released from the surface of the plasmonic material (gold). By reducing the outer diameter of the optical fiber and creating a D-shape, the generation of the evanescent field will be enhanced. The surface plasmon wave is generated by interacting with the evanescent field and the metal surface. As the surface plasmon wave transfers forward, a frequency matching occurs between the fundamental mode and SPP mode. The y-polarization core fundamental mode and x-polarization core fundamental mode, and SPR mode in the sensing layer were examined as illustrated in Figure 4.
These images show that the energy of the fundamental mode under x- and y-polarization is not solely confined to the core, but a portion of this energy transfers to the surface of the nanomaterial, made of Au Hemisphere structures. This energy then facilitates the coupling of the fiber fundamental core mode and SPR mode, which may lead to strong electromagnetic field coupling that is likely to enhance the sensor's sensitivity.

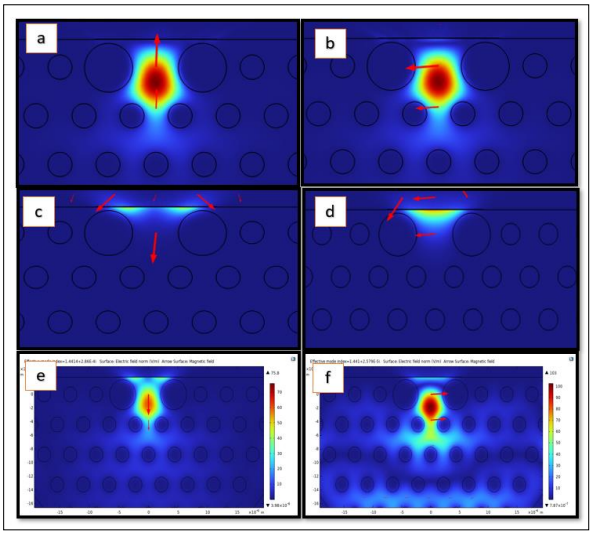

Fig. 4: The electric field distributions of (a) fundamental y-polarized mode, (b) fundamental x-polarized mode, (c) SPP y-polarized mode, (d) SPP x-polarized mode, (e) phase matching mode for y-polarized, and (f) phase matching mode for x-polarized

Both y- and x-polarization fundamental modes exist in the core, with birefringence on the order of 10^{-4} which higher than that of conventional PM fibers. This feature makes PM-PCF valuable in fiber optic sensing, and other advanced optical applications where precise control over polarization is required. In this study, both y- and x-polarized modes are considered. Two resonance peaks are observed in the spectra of confinement loss because of the resonance coupling of two distinct higher-order SP modes with the fundamental core mode of the D-shape-PM-PCF. Figure 5 illustrates the dispersion relation of the y-polarized fundamental mode and SPP mode loss spectra for the analyte's RI equal to 1.34 RIU.

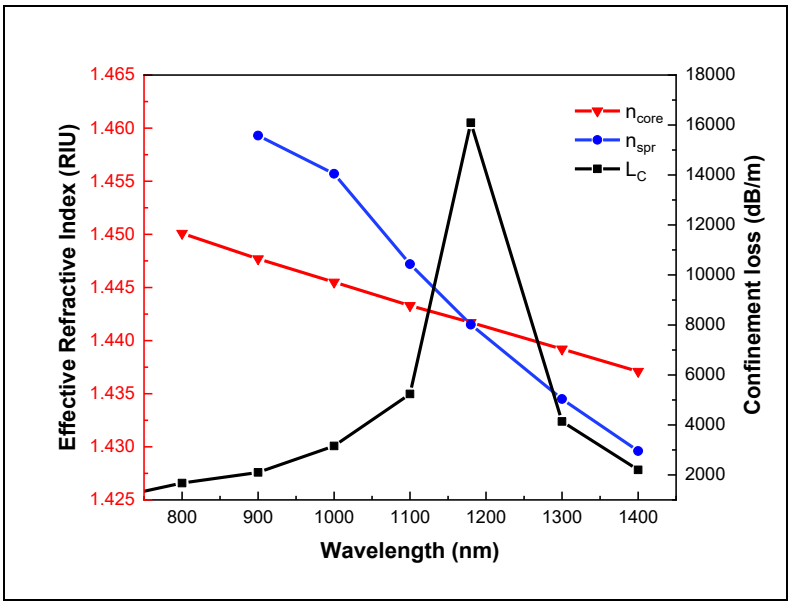

Fig. 5: The Dispersion relationship of the y-polarized core-guided mode, SPP mode, and loss spectra, for analyte RI = 1.34 RIU

The y-polarization loss curve, which initially increases with wavelength, reaches a maximum peak at the resonant wavelength and decreases with further wavelength increase. The resonant wavelength is detected at 1180nm, where the peak coincides with the intersection of the two dispersion curves. This intersection, where the effective RI of the core mode and refractive index of the SPP mode of the sensor are equal, signifies the phase-matching coupling phenomenon.

The confinement loss of the fundamental core mode dependence on wavelength for various analyte refractive indices in both x-polarization and y-polarization are depicted in Figure 6. This figure illustrates how the wavelength sensitivity varies with the analyte's refractive index (RI) for both x- and y-polarization modes. The sensitivity changes in response to variations in refractive index and peak wavelength. According to Equation (4), sensitivity rises if the RI analyte variation decreases or the peak wavelength variation increases, and vice versa. The scanning wavelength is chosen before and after 1550nm, this is because in plasmonic sensors different modes of surface plasmon polaritons can be excited at various wavelengths. Also, the dispersion properties of gold plasmonic material change significantly with wavelength. Gold has distinct plasmonic responses in the visible (around 500 nm) and near-infrared (NIR) regions (around 1100 nm). The material's dielectric function, which varies with wavelength, can lead to different resonance conditions at these wavelengths. This resonance wavelength could be shifted due to the changing of the surrounding refractive index [23].

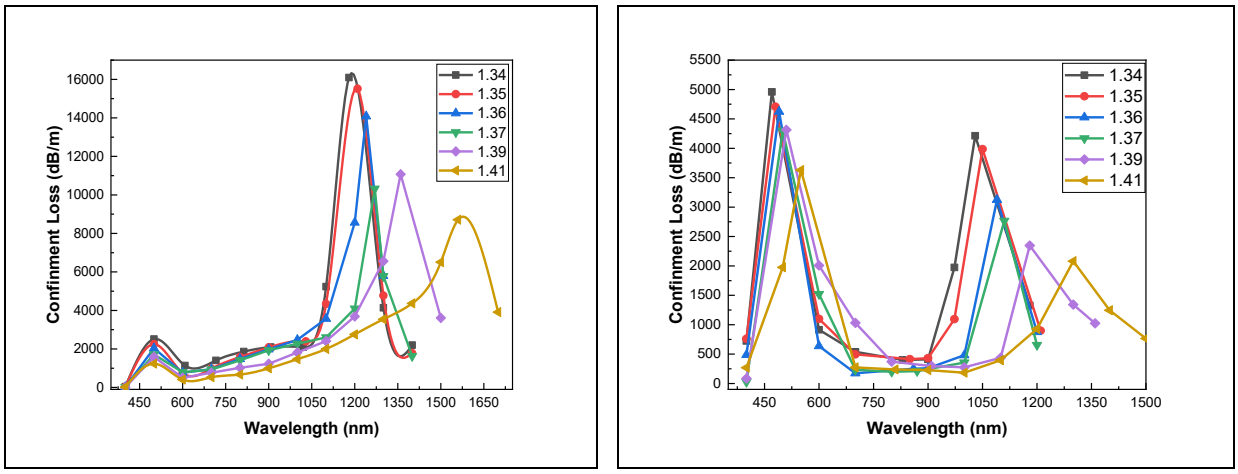

Fig. 6: Confinement loss spectra of different analyte refractive indices (a) for y- y-polarization, (b) for x-polarization

From the dispersion relation of the fundamental core in the y-polarization mode and plasmonic modes shown in Figure 6, two loss peaks were observed. The reason behind the appearance of two peaks could be due to the interaction of different SPP modes with the core fundamental mode. Also, this multiple peaks appearance could be due to the complexity of the plasmonic layer shape [49]. These peaks shift towards longer wavelengths, and their intensity decreases as the RI of the analyte increases for the 2nd peak of y-polarization and both peaks of x-polarization, as clear in Figure 6. The loss curve amplitude in the 1st peak of y-polarization increases as the RI of analytes decreases [50]. These behaviors provide ample information about the variation in the analyte RI.

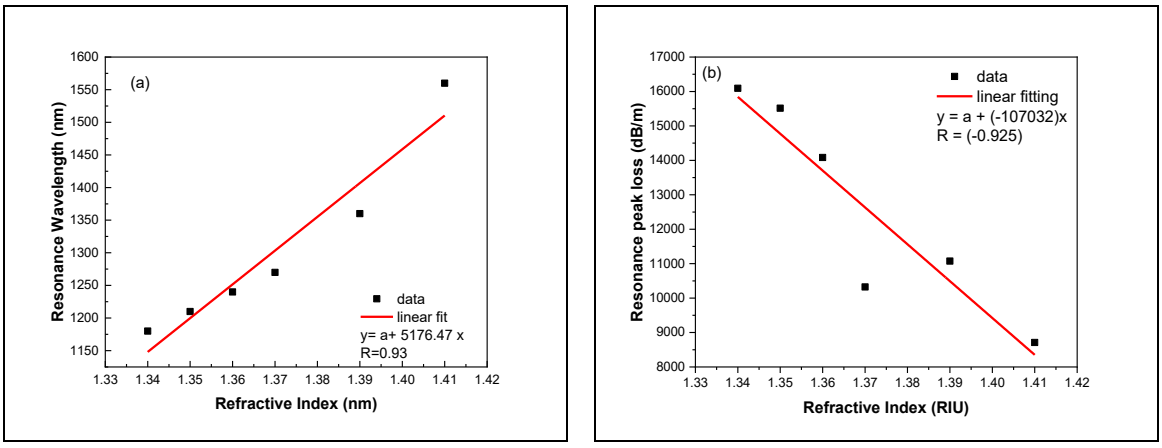

Fig.7: A linear fit that represented (a) the resonance wavelengths and (b) the loss peak intensity, as a function of the analyte RI. (For Y-polarization)

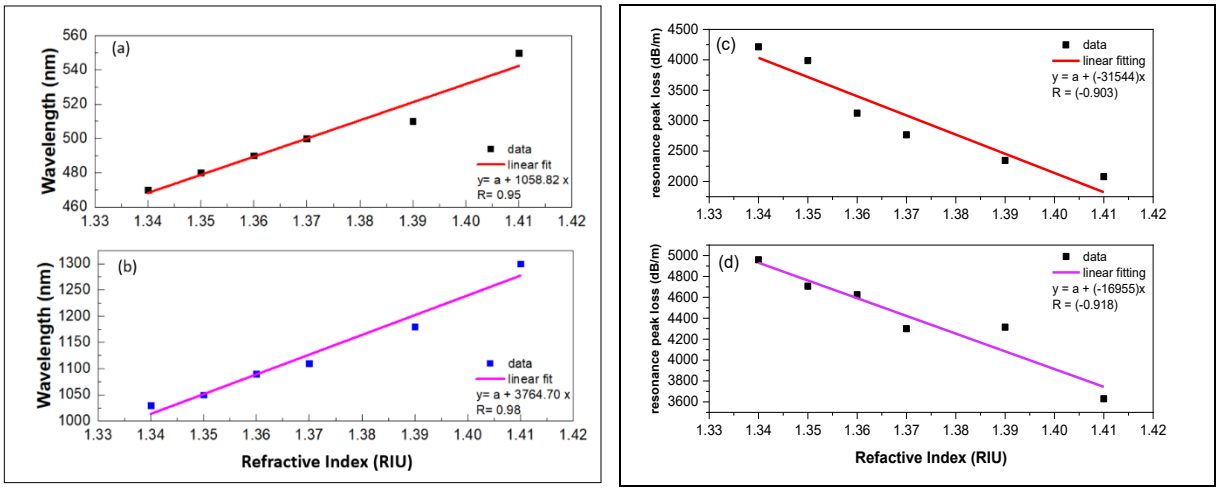

Fig.8: A linear fit that represented (a, b) the resonance wavelengths and (c, d) the loss peak intensity, as a function of the analyte RI for P1 and P2. (For X-polarization)

Variation in the analyte's RI causes a shift in the resonance wavelength because it affects the distribution of the sensor's electric field. The decrease in peak intensity results from the increased surface plasmon resonance mode attenuation as the analyte's refractive index rises. Combining polarization-maintaining photonic crystal fibers with surface plasmon resonance principles leads to the design of sensors that are highly sensitive to variation in RI and maintain the polarization state of light, ensuring precise and stable measurements.

A linear relationship exists between both the resonance wavelength and peak intensity with the analyte's refractive index within the range of 1.34 RIU to 1.41 RIU for Y-polarization and X-polarization mode, as depicted in Figures 7 and 8.

These figures demonstrate that the two resonance loss peaks exhibit high sensitivity to the filled analyte's refractive index (1.34-1.41) RIU. The loss peak will continuously shift to longer wavelengths as the analyte's RI rises, enabling the detection of the analyte's RI through analysis of the loss spectrum. So, the D-PM-PCF-SPR structure is suitable for refractive index sensing applications. The relationship between the analyte's refractive index and the SPR wavelength for y-polarization for the 2nd peak is expressed by y=a+ (5.176) x which shows high linearity R=0.93.

The relationship between the analyte's refractive index and the SPR wavelength for x-polarization for both peaks are expressed by y=a+ (1.058) x for 1st peak, and y=a+(3.764) x for 2nd peak, respectively. Both peaks have high linearity R=0.95 for 1st peak and R=0.98 for 2nd peak, respectively.

For RI values ranging from 1.34 to 1.41, the maximum wavelength sensitivity of the peak is 5176 nm/RIU, and the spectral resolution for this sensor is 1.93 x 10^{-5} RIU, for y-polarization. For x-polarization and the same range of RI, the maximum sensitivity of the 1st and 2nd peaks is 1058 nm/RIU and 3764 nm/RIU, respectively. The spectral resolution for the 1st and 2nd peaks is 9.45x 10^{-5} RIU and 2.65x 10^{-5} RIU, respectively.

The figure of merit (FOM) is regarded as a crucial factor for assessing the sensor performance and quality because it measures the sensor sensitivity and efficiency to detect minor variations in the surrounding

refractive index. FWHM measures the width of a sensor's response curve at half its peak, characterizing its resolution or bandwidth. A higher FOM indicates an improved signal-to-noise ratio for the sensor and thus reducing signal noise. Table (3) presents the FOM values for different refractive indices RIs in both x- and y-polarization. The proposed SPR sensor has an FWHM of 50.99 at n_a of 1.37 and a maximum FOM of 101.5 for the y-polarization mode.

Table 3 illustrates the FOM in (RIU^{-1}) calculation for the proposed sensor

n_a (RIU)	FOM (RIU^{-1})		
	X-polarization mode		Y-polarization mode
	P1	P2	P2
1.34	13.5	34.2	43.5
1.35	13.6	27.7	41.4
1.36	11.6	64	63.1
1.37	12.9	46.7	101.5
1.39	10.3	50.8	32.4
1.41	9.5	24	25

Table 4 provides a comparative analysis of the maximum sensitivity and spectral resolution of the proposed sensor and others in recent published work.

Table 4. Performance comparison with other SPR fiber-based sensors

Ref. No.	Type and shape of the plasmonic material	WS (nm/RIU)	Resolution (RIU)	Detection range (RIU)
[51]	Gold / thin layer	2200	3.75×10^{-5}	1.33 - 1.36
[27]	Graphene / thin layer	2000	5×10^{-5}	1.331 - 1.339
[52]	Gold and molybdenum disulfide / thin layers	5100	1.96×10^{-5}	1.19 - 1.40
[39]	Gold / Grating	994.5	2.03×10^{-6}	1.33 - 1.37
[53]	Gold / Nanoparticles	3157.98	3.16×10^{-5}	1.281- 1.39
[54]	Gold / thin layer	1000	1×10^{-4}	1.33 - 1.37
This work	Gold / Hemisphere structure	For x-polarization, P1: **1058** P2: **3764** For y- polarization, P2: **5176**	9.45×10^{-5} 2.65×10^{-5} 1.93×10^{-5}	1.34 – 1.41

5. Conclusion

In conclusion, this study presents a new SPR-based PM-PCF sensor. Due to its chemical stability, gold was utilized as a plasmonic material with hemispherical structures on the surface of the D-shaped sensor to induce the SPR effect. Numerical analyses were conducted using Finite Element Method (FEM) in the frequency domain. Our suggested design offers a high wavelength sensitivity (WS) of 5176 nm/RIU and the spectral resolution for this sensor is 1.93×10^{-5} RIU, for y-polarization. For x-polarization, the wavelength sensitivity of the 1st and 2nd peaks are 1058 nm/RIU and 3764 nm/RIU, respectively. The spectral resolution for the 1st and 2nd peaks is 9.45×10^{-5} RIU and 2.65×10^{-5} RIU, respectively in the high sensing range of 1.34 to 1.41 RIU. Y-polarization was used for better performance of the proposed sensor,

due to high confinement loss and Figure of Merit (FOM). The sensor demonstrates excellent spectral resolution allowing for precise measurement of refractive index changes within the specified range. These findings could affect highly sensitive and high-resolution refractive index sensing applications, such as biosensors and environmental monitoring systems.

References

[1] W. Luo, B. Liu, J. Liu, T. Wu, Q. Liu, M.-Y. Wang, *et al.*, "Tapered side-polished microfibre sensor for high sensitivity hCG detection," *IEEE Sensors Journal*, vol. 22, pp. 7727–7733, 2022.
[2] H. A. Mohammed, S. A. Rashid, M. H. A. Bakar, S. B. A. Anas, M. A. Mahdi, and M. H. Yaacob, "Fabrication and characterizations of a novel etched-tapered single mode optical fiber ammonia sensors integrating PANI/GNF nanocomposite," *Sensors and Actuators B: Chemical*, vol. 287, pp. 71–77, 2019.
[3] V. T. Huong, N. T. T. Phuong, N. T. Tai, N. T. An, V. D. Lam, D. H. Manh, *et al.*, "Gold nanoparticles modified a multimode clad-free fiber for ultrasensitive detection of bovine serum albumin," *Journal of Nanomaterials*, vol. 2021, p. 5530709, 2021.
[4] H. J. Taher, "The influence of no-core fiber length on the sensitivity in fiber optic strain sensor," *Iraqi Journal of Laser*, vol. 20, pp. 13–20, 2021.
[5] Y. Liu, H. Chen, Y. Guo, M. Wang, X. Meng, X. Jing, *et al.*, "Ultra-high sensitivity plasmonic sensor based on D-shaped photonic crystal fiber with offset-core," *Optik*, vol. 221, p. 165309, 2020.
[6] D. M. Kim, J. S. Park, S.-W. Jung, J. Yeom, and S. M. Yoo, "Biosensing applications using nanostructure-based localized surface plasmon resonance sensors," *Sensors*, vol. 21, p. 3191, 2021.
[7] M. Elsherif, A. E. Salih, M. G. Muñoz, F. Alam, B. AlQattan, D. S. Antonysamy, *et al.*, "Optical fiber sensors: Working principle, applications, and limitations," *Advanced Photonics Research*, vol. 3, p. 2100371, 2022.
[8] C. Ma, D. Peng, X. Bai, S. Liu, and L. Luo, "A review of optical fiber sensing technology based on thin film and Fabry–Perot cavity," *Coatings*, vol. 13, p. 1277, 2023.
[9] M. R. Islam, M. M. Ali, M.-H. Lai, K.-S. Lim, and H. Ahmad, "Chronology of Fabry–Perot interferometer fiber-optic sensors and their applications: a review," *Sensors*, vol. 14, pp. 7451–7488, 2014.
[10] Y.-J. Rao, Z.-L. Ran, and Y. Gong, *Fiber-Optic Fabry–Perot Sensors: An Introduction*, CRC Press, 2017.
[11] F. Xue, Y. Yao, P. Xu, J. Luo, L. Li, L. Zhang, *et al.*, "Ultra-high sensitive refractive index sensor based on D-shaped photonic crystal fiber with graphene-coated Ag-grating," *Heliyon*, vol. 9, 2023.
[12] C. Liu, J. Lü, W. Liu, F. Wang, and P. K. Chu, "Overview of refractive index sensors comprising photonic crystal fibers based on the surface plasmon resonance effect," *Chinese Optics Letters*, vol. 19, p. 102202, 2021.
[13] H. Huang, Z. Zhang, Y. Yu, L. Zhou, Y. Tao, G. Li, *et al.*, "A highly magnetic field sensitive photonic crystal fiber based on surface plasmon resonance," *Sensors*, vol. 20, p. 5193, 2020.
[14] R. B. Schasfoort, *Handbook of Surface Plasmon Resonance*, Royal Society of Chemistry, 2017.
[15] D. Wang, W. Li, Q. Zhang, B. Liang, Z. Peng, J. Xu, *et al.*, "High-performance tapered fiber surface plasmon resonance sensor based on the graphene/Ag/TiO_2 layer," *Plasmonics*, vol. 16, pp. 2291–2303, 2021.
[16] P. Bing, Q. Liu, G. Wu, S. Yuan, Z. Li, H. Du, *et al.*, "A plasmonic sensor based on D-shaped dual-core microchannel photonic crystal fiber," *Plasmonics*, vol. 17, pp. 1471–1478, 2022.
[17] R. Zakaria, M. Mahbub, and C. Lim, "Studies of surface plasmon resonance effect on different metallic layers of silver (Ag) and copper (Cu) with molybdenum trioxide (MoO_3) for formaldehyde sensor," *Results in Optics*, vol. 11, p. 100374, 2023.
[18] M. R. Sardar and M. Faisal, "Numerical analysis of highly sensitive twin-core, gold-coated, D-shaped photonic crystal fiber based on surface plasmon resonance sensor," *Sensors*, vol. 23, p. 5029, 2023.
[19] D. Kumar, M. Khurana, M. Sharma, and V. Singh, "Analogy of gold, silver, copper and aluminium based ultra-sensitive surface plasmon resonance photonic crystal fiber biosensors," *Materials Today: Proceedings*, 2023.
[20] A. Khaleque, E. G. Mironov, J. H. Osório, Z. Li, C. M. Cordeiro, L. Liu, *et al.*, "Integration of bow-tie plasmonic nano-antennas on tapered fibers," *Optics Express*, vol. 25, pp. 8986–8996, 2017.

[21] S. A. S. Sunny, T. Ahmed, S. M. Hiam, and A. K. Paul, "Highly sensitive externally metal coated plasmonic refractive index sensor based on photonic crystal fiber," Optik, vol. 243, p. 167482, 2021.
[22] L. F. Abdulrazak, M. B. Hossain, M. S. Islam, A. F. Alkhateeb, I. M. Mehedi, S. Roy, et al., "Plasmonic sensor based on microstructure PCF: performance analysis with outside detecting approach," Optical and Quantum Electronics, vol. 54, p. 58, 2022.
[23] C. Caucheteur, T. Guo, and J. Albert, "Review of plasmonic fiber optic biochemical sensors: improving the limit of detection," Analytical and Bioanalytical Chemistry, vol. 407, pp. 3883–3897, 2015.
[24] M. Tu, T. Sun, and K. Grattan, "Optimization of gold-nanoparticle-based optical fibre surface plasmon resonance (SPR)-based sensors," Sensors and Actuators B: Chemical, vol. 164, pp. 43–53, 2012.
[25] Q. Wang, X. Jiang, L.-Y. Niu, and X.-C. Fan, "Enhanced sensitivity of bimetallic optical fiber SPR sensor based on MoS_2 nanosheets," Optics and Lasers in Engineering, vol. 128, p. 105997, 2020.
[26] S. Cai, H. Pan, Á. González-Vila, T. Guo, D. C. Gillan, R. Wattiez, et al., "Selective detection of cadmium ions using plasmonic optical fiber gratings functionalized with bacteria," Optics Express, vol. 28, pp. 19740–19749, 2020.
[27] A. K. Paul, M. A. Mollah, M. Z. Hassan, N. Gomez-Cardona, and E. Reyes-Vera, "Graphene-coated highly sensitive photonic crystal fiber surface plasmon resonance sensor for aqueous solution: Design and numerical analysis," in Photonics, p. 155, 2021.
[28] Y. Fei, B. Luo, M. An, T. Hu, W. Lin, and H. Jia, "Highly sensitive surface plasmon resonance refractive index sensor based on D-shaped dual-core photonic crystal fiber with ITO film," Plasmonics, pp. 1–15, 2023.
[29] S. Jain, K. Choudhary, and S. Kumar, "Novel materials–based photonic crystal fiber sensor for biomedical applications," Plasmonics, pp. 1–14, 2023.
[30] W. Zhou, X. Qin, M. Lv, L. Qiu, Z. Chen, and F. Zhang, "Design of plasmonic photonic crystal fiber for highly sensitive magnetic field and temperature simultaneous measurement," Micromachines, vol. 14, p. 1684, 2023.
[31] Q. Liu, S. Hou, J. Dong, J. Lei, G. Wu, and Z. Yan, "D-shaped microstructure fiber temperature sensor based on surface plasmon resonance," Japanese Journal of Applied Physics, vol. 62, p. 096002, 2023.
[32] B. S. Boruah and R. Biswas, "Localized surface plasmon resonance based U-shaped optical fiber probe for the detection of Pb^{2+} in aqueous medium," Sensors and Actuators B: Chemical, vol. 276, pp. 89–94, 2018.
[33] C. Teng, P. Shao, S. Li, S. Li, H. Liu, H. Deng, et al., "Double-side polished U-shape plastic optical fiber based SPR sensor for the simultaneous measurement of refractive index and temperature," Optics Communications, vol. 525, p. 128844, 2022.
[34] L.-X. Kong, Y.-X. Zhang, W.-G. Zhang, Y.-S. Zhang, T.-Y. Yan, P.-C. Geng, et al., "Lab-on-tip: Protruding-shaped all-fiber plasmonic microtip probe toward in-situ chem-bio detection," Sensors and Actuators B: Chemical, vol. 301, p. 127128, 2019.
[35] J. Wang, W. Liu, L. Yang, J. Lv, Q. Yin, Q. Liu, et al., "Symmetrical dual D-shape fiber for waveguide coupled surface plasmon resonance sensing," Optik, vol. 287, p. 171162, 2023.
[36] X. Meng, J. Li, Y. Guo, S. Li, Y. Wang, W. Bi, et al., "An optical-fiber sensor with double loss peaks based on surface plasmon resonance," Optik, vol. 216, p. 164938, 2020.
[37] F. Mumtaz, M. Roman, B. Zhang, L. G. Abbas, M. A. Ashraf, M. A. Fiaz, et al., "A simple optical fiber SPR sensor with ultra-high sensitivity for dual-parameter measurement," IEEE Photonics Journal, vol. 14, pp. 1–7, 2022.
[38] H. P. Li, J. Ruan, X. Li, Q. Q. Zhang, J. J. Chen, T. He, et al., "High-sensitivity refractive index sensor of arc-shape photonic crystal fiber based on surface plasmon resonance," Progress in Electromagnetics Research C, vol. 137, pp. 29–38, 2023.
[39] Y. Ying, Y. Xia, S. Cheng, D. Shan, Z. Gao, G. Si, et al., "High performance dual-core D-shaped PCF refractive index sensor coated with gold grating," in Photonics, p. 473, 2023.
[40] L.-Q. Chen, Y.-C. Wu, Y. Liu, H. Y. Cai, and J. Liu, "Highly sensitive dual-function sensor for refractive index and temperature using D-shaped microchannel photonic crystal fiber," Optics Express, vol. 32, pp. 12405–12418, 2024.
[41] M. Koshiba, Y. Tsuji, and M. Hikari, "Finite element beam propagation method with perfectly matched layer boundary conditions," IEEE Transactions on Magnetics, vol. 35, pp. 1482–1485, 1999.

[42] X. Yan, R. Fu, T. Cheng, and S. Li, "A highly sensitive refractive index sensor based on a V-shaped photonic crystal fiber with a high refractive index range," Sensors, vol. 21, p. 3782, 2021.
[43] M. R. Islam, M. M. I. Khan, F. Mehjabin, J. A. Chowdhury, M. Islam, A. J. Yeasir, et al., "Design of a dual spider-shaped surface plasmon resonance-based refractometric sensor with high amplitude sensitivity," IET Optoelectronics, vol. 17, pp. 38–49, 2023.
[44] X. Chen, L. Xia, and C. Li, "Surface plasmon resonance sensor based on a novel D-shaped photonic crystal fiber for low refractive index detection," IEEE Photonics Journal, vol. 10, pp. 1–9, 2018.
[45] W. Li, Y. Chen, J. Xu, M. Jiang, and H. Zou, "A dual-core surface plasmon resonance-based photonic crystal fiber sensor for simultaneously measuring the refractive index and temperature," Crystals, vol. 13, p. 972, 2023.
[46] H. Qiu, W. Li, C. Zhu, J. Xu, J. Li, and G. Bai, "A high-sensitivity D-shaped photonic crystal fiber surface plasmon resonance sensor for low refractive index detection," Journal of Optics, pp. 1–9, 2023.
[47] Y. Li, H. Chen, H. Li, Z. Gao, X. Fan, and Q. Chen, "Highly sensitive methane gas sensor based on Au/UVCFS films coated D-shaped photonic crystal fiber," Physica Scripta, vol. 98, p. 065533, 2023.
[48] A. K. Paul, A. K. Sarkar, A. B. S. Rahman, and A. Khaleque, "Twin core photonic crystal fiber plasmonic refractive index sensor," IEEE Sensors Journal, vol. 18, pp. 5761–5769, 2018.
[49] Z.-K. Fan, S.-B. Fang, S.-G. Li, and Z.-Y. Wei, "Refractive index sensor based on high-order surface plasmon resonance in gold nanofilm coated photonic crystal fiber," Chinese Physics B, vol. 28, p. 094209, 2019.
[50] K. Ahmed, M. A. AlZain, H. Abdullah, Y. Luo, D. Vigneswaran, O. S. Faragallah, et al., "Highly sensitive twin resonance coupling refractive index sensor based on gold-and MgF_2-coated nano metal films," Biosensors, vol. 11, p. 104, 2021.
[51] M. R. Hasan, S. Akter, A. A. Rifat, S. Rana, and S. Ali, "A highly sensitive gold-coated photonic crystal fiber biosensor based on surface plasmon resonance," in Photonics, p. 18, 2017.
[52] X. Guo, Y. Wang, T. Sang, G. Yang, and Q. Yao, "SPR sensor based on a concave photonic crystal fiber structure with MoS_2/Au layers," Materials, vol. 16, p. 5523, 2023.
[53] M. A. Fakhri, E. T. Salim, S. M. Tariq, R. K. Ibrahim, F. H. Alsultany, A. A. Alwahib, et al., "A gold nanoparticles coated unclad single mode fiber-optic sensor based on localized surface plasmon resonance," Scientific Reports, vol. 13, p. 5680, 2023.
[54] A. A. Rifat, G. A. Mahdiraji, Y. Shee, M. J. Shawon, and F. M. Adikan, "A novel photonic crystal fiber biosensor using surface plasmon resonance," Procedia Engineering, vol. 140, pp. 1–7, 2016.
[55] F. J. Moaen and H. R. Humud, "Raman scattering enhancement by silver nanostructures prepared by electrical exploding wire technique," Iraqi Journal of Science, pp. 2017–2024, 2022.

متحسس عالي الحساسية لمعامل الانكسار المعتمد على بلازمونات مزدوجة القمة في الليف البصري الفوتوني مديم الاستقطاب ذو الشكل D والمغطى بهياكل ذهب نانوية

سعاد صاحب هندال[2،1] * ، زينب فاضل مهدي[1] ، أسيل إبراهيم محمود [2]

[1]معهد الليزر للدراسات العليا/ جامعة بغداد
[2]هيئة البحث العلمي / وزارة التعليم العالي والبحث العلمي

البريد الالكتروني للباحث*: suad.saheb2101p@ilps.uobaghdad.edu.iq

الخلاصة: يدرس هذا البحث متحسس تأثير رنين البلازمون السطحي (SPR) استنادًا إلى الألياف البلورية الفوتونية المديمة للاستقطاب(PM-PCF) بشكل D باستخدام طريقة العناصر المحددة. وباستخدام عنصر الذهب (Au) كمادة بلازمونية

وبتراكيب نصف كروية لها نصف قطر يبلغ 50 نانومتر على سطح المتحسس ذو الشكل D لإنتاج تأثير الرنين البلازموني السطحي(SPR) ، مما يتيح للمتحسس اكتشاف التغيرات في معامل ر انكسار العنصر المحيط. ستتغير قمم الانحلال عندما تتغير معامل انكسار العنصر المطلوب الكشف عنه، مما يؤدي إلى زحزحة معين في ذروة الفقد. حيث تم ملاحظة قمتي رنين، الأولى في الجزء المرئي من الطيف، والثانية في منطقة الأشعة تحت الحمراء القريبة. التصميم المقترح يُظهر حساسية عالية للطول الموجي (WS) ، حيث بلغت (5176 نانومتر/وحدة معامل الانكسار) والدقة الطيفية لهذا المتحسس هي (1.93 x 10^{-5} وحدة معامل الانكسار)، لأنماط المحور الصادي للاستقطاب. وبالنسبة لأنماط الاستقطاب للمحور السيني، فإن الحساسية القصوى للقمة الأولى والثانية هي (1058 نانومتر/ وحدة معامل الانكسار) و (3764 نانومتر/وحدة معامل الانكسار)، على التوالي. الدقة الطيفية للقمة الأولى والثانية هي (9.45 x 10^{-5} وحدة معامل الانكسار) و (2.65 x 10^{-5} وحدة معامل الانكسار), على التوالي وفي ضمن مدى معاملات الانكسار من 1.34 إلى 1.41 وحدة معامل انكسار. تُظهر النتائج أن هذا التصميم حَسن قدرة التحسس على كشف التغير في معاملات الانكسار. التصميم المقترح للمتحسس يتصف بحساسية ودقة وخطية عالية، وهي نتيجة واعدة يمكن استخدامها في مراقبة البيئة والكشف البيولوجي والمتحسسات الفيزيائية والتحليل الكيميائي.